Confocal reflectance mosaicing of basal cell carcinomas in Mohs surgical skin excisions

Yogesh G. Patel
Kishwer S. Nehal
Memorial Sloan-Kettering Cancer Center
160 East 53rd Street
Dermatology Service, Floor #2
New York, New York 10022

Iana Aranda
Yongbiao Li
Memorial Sloan-Kettering Cancer Center
1275 York Avenue
Research Engineering Laboratory, Room RRL 551
New York, New York 10021

Allan C. Halpern
Milind Rajadhyaksha
Memorial Sloan-Kettering Cancer Center
160 East 53rd Street
Dermatology Service, Floor #2
New York, New York 10022

Abstract. Precise removal of basal cell carcinomas (BCCs) with minimal damage to the surrounding normal skin is guided by the examination of frozen histology of each excision during Mohs surgery. The preparation of frozen histology is slow, requiring 20 to 45 min per excision. Confocal reflectance mosaicing may enable rapid detection of BCCs directly in surgical excisions, with minimal need for frozen histology. Soaking the excisions in acetic acid rapidly brightens nuclei and enhances BCC-to-dermis contrast. Clinically useful concentrations of acetic acid from 10 to 1% require 30 s to 5 min, respectively. A tissue fixture precisely controls the stability, flatness, tilt, and sag of the excisions, which enables mosaicing of 36×36 images to create a field of view of 12×12 mm. This simulates a $2\times$ magnification view in light microscopes, which is routinely used by Mohs surgeons to examine frozen histology. Compared to brightfield, cross-polarization enhances contrast and detectability of BCCs in the papillary dermis but not in the reticular dermis. Comparison of mosaics to histology shows that nodular, micronodular, and superficial BCCs are easily detected. However, infiltrative and sclerosing BCCs tend to be obscured within the surrounding bright dermis. The mosaicing method currently requires 9 min, and thus may expedite Mohs surgery. [DOI: 10.1117/1.2750294]

Keywords: confocal optics; basal cell carcinomas; Mohs surgery; acetowhitening.

Paper 06143RR received Jun. 8, 2006; revised manuscript received Feb. 2, 2007; accepted for publication Feb. 5, 2007; published online Jun. 27, 2007.

1 Introduction

Among skin malignancies, basal cell carcinoma (BCC) is the most common, occurring at an estimated rate of 800,000 cases in the United States every year.[1] BCCs are tumors most commonly occurring on sun-exposed areas of the body such as the face or head, and often on or near the nose, eyes, ears, or mouth. Because of this occurrence in high-risk anatomical areas, BCCs require precise excision with minimal loss of the surrounding normal tissue, and are effectively treated with Mohs micrographic surgery.[2,3] Mohs surgery involves curetting of the gross tumor, followed by continued thin excisions of skin, which are immediately processed for frozen pathology. The surgeon examines the pathology sections for the presence of BCC in the peripheral and deep margins of the excision. Excisions are repeatedly performed and examined until the last section shows no residual features of BCC. This is followed by closure of the excised wound. Mohs surgery generally requires one to two excisions, with preparation of frozen sections and examination requiring 20 to 45 min per excision.[4] During the preparation of frozen pathology sections, the patient must wait under local anesthesia with an open wound. Mohs surgery thus requires a total visit time of 1 to 2 h per patient. For large and complex cases, several excisions may be required, and the total visit time may extend to several hours.

Optical imaging methods are being developed that may enable rapid detection of BCCs directly and noninvasively in surgical skin excisions, minimize the need for frozen pathology, and expedite Mohs surgery. The optical methods include confocal reflectance microscopy,[4–8] optical coherence tomography,[9] multispectral fluorescence polarization using methylene blue and toluidine blue dyes,[10,11] terahertz imaging,[12–14] near-IR spectroscopy,[15] Raman spectroscopy,[16] fluorescence microscopy following staining with amino levulinic acid-induced protoporphyrin IX,[17–20] and autofluorescence.[21] In confocal microscopy, a point source of light illuminates a 3-D spot or voxel within the tissue. In reflectance mode of contrast, the light that is backscattered from the voxel is collected through an optically conjugate aperture (pinhole) onto a detector. The pinhole rejects multiply scattered out-of-focus light while allowing only the in-focus light from the voxel to reach the detector. Light that is detected from a voxel results in a pixel at the detector output. By scanning the voxel in two dimensions, a pixel-by-pixel image of a thin plane, or an optical section, within the tissue is noninvasively produced.

In previous research, we demonstrated detection of BCCs with confocal reflectance microscopy in skin excisions that

Address all correspondence to: Milind Rajadhyaksha, Memorial Sloan-Kettering Cancer Center, 160 East 53rd Street, Dermatology Service, Room 230, New York, New York 10022; Tel: 212–610–0832; Fax: 212–308–0739; E-mail: rajadhym@mskcc.org.

1083-3668/2007/12(3)/034027/10/$25.00 © 2007 SPIE

are up to 10 mm in size.[5] The contrast of BCCs relative to the surrounding dermis was enhanced by "acetowhitening": soaking skin excisions in acetic acid of concentration 5% for 3 min. The mechanism of acetowhitening was explained by the condensation of chromatin which increases backscattering of light and results in a bright white appearance of the nuclei, making them more easily detectable.[4,5,22] Light backscatter from the condensed chromatin was found to be significantly depolarized, whereas that from the surrounding dermis retained the polarization of the illumination light. Thus, in brightfield images, both the nuclei and the surrounding dermis appear bright such that the BCCs appear with relatively low contrast. However, when illuminated with linearly polarized light and detected through a crossed polarizer, the nuclei appeared bright in the images whereas the surrounding dermis appeared dark. Consequently, BCC nuclei-to-dermis contrast appear enhanced in cross-polarized images, compared to that in brightfield images.

Rapid detection of BCCs during Mohs surgery will require rapid acetowhitening with short soaking times followed by rapid imaging of large (typically 10 to 20 mm) excisions. We report the results of a preclinical study to determine nuclear brightening and detectability of BCCs using acetic acid concentrations between 1 and 10% and soaking times between 30 s to 5 min that would be useful in clinical settings. Advances in instrumentation are described, particularly, a mechanical fixture to precisely mount large excisions and creation in software of image mosaics over large areas of tissue. Visual correlations of confocal reflectance mosaics to the corresponding frozen histology sections at varying fields of view are shown. Comparison of cross-polarized to brightfield contrast is further described.

2 Materials and Methods

2.1 *Excised Tissue Collection*

Skin excisions from Mohs surgeries were obtained from the Mohs Surgery Unit in the Dermatology Service at Memorial Sloan-Kettering Cancer Center (MSKCC) under Human Tissue Utilization Committee (HTUC) approval. For each excision, the Mohs technician usually prepares three to four frozen sections, with each section being approximately 5 to 6 μm thick. After the Mohs surgeon has obtained and evaluated the frozen sections for histology, the remnants of each excision are usually discarded. All discarded excisions were collected at the end of the day, after the completion of Mohs surgeries. Thus, our research did not compromise the standard Mohs surgical and pathology procedures, and did not affect routine patient care. Fresh excisions of normal skin were also collected. Such excisions of redundant normal skin, also referred to as "dog ears" because of their shape, is sometimes performed to optimize surgical wound closure and maximize cosmetic-reconstructive outcome.

2.2 *Excised Tissue Preparation*

The collected excision specimens were frozen in the embedding medium that is used in preparing histology sections. Each excision was thawed, removed from the embedding medium, washed with lukewarm water for several minutes, placed in a vial of potassium phosphate monobasic-sodium hydroxide buffer solution (PBS) and then refrigerated. The excisions were living, as confirmed by viability staining with fluorescein diacetate and fluorescence-imaging of the subsequent fluorescein-labeled cytoplasm (unpublished data).

The confocal imaging of each excision was performed in two stages: before acetowhitening (control) and after. For the control, we imaged the excision from the PBS solution. The excision was then acetowhitened by soaking in acetic acid for a set time and again imaged. A total of 125 excisions were imaged in this study. The tested concentrations of acetic acid were 10, 5, 3, 2, and 1%, with soaking times of 5, 3, 2, and 1 min, and 30 s. For each combination of concentration and time, 5 excisions were imaged to test repeatability, resulting in the total of 125 excisions.

The skin excisions were typically of size 10 to 20 mm and thickness 2 mm, such that the tissue volume was no more than 1 ml (considering that 60 to 70% of the content of tissue is water). The excisions were soaked in 15 ml of acetic acid. Thus, for the acetowhitening, the ratio of the volume of acetic acid to the volume of tissue was 15:1. The low concentrations of acetic acid that were used do not affect the compliance of the tissue and do not affect the subsequent sectioning and staining for frozen histology. This was verified in the initial studies.[4,5] (Low-concentration acetic acid, whenever used for acetowhitening on skin or mucosa, can be rinsed out of the tissue prior to preparation of frozen histology. Note, however, that at much higher concentrations such as 50%, acetic acid fixes tissue. High-concentration acetic acid is, in fact, used as a fixative for several tissues. In bone tissue, for example, acetic acid facilitates the removal of calcified material, which is required prior to fixation.)

2.3 *Confocal Microscope Instrumentation*

The imaging was performed with a modified laboratory breadboard version of a commercial reflectance confocal microscope (VivaScope 2000, Lucid Inc., Rochester, New York) that is designed specifically for imaging fresh tissue excisions *ex vivo*. The design and instrumentation details were reported earlier.[4,5] The illumination is with a near-IR diode laser at wavelength of 830 nm and low power of about 1 to 5 mW on the tissue. The objective lens is a 30×, 0.9 numerical aperture (NA) water immersion (StableView, Lucid Inc., Rochester, New York) that was custom-made to image through a 1-mm-thick glass window. Standard 1-mm-thick microscope cover slides were used as the glass window (part number 12-550A, Fisher Scientific, Pittsburgh, Pennsylvania). The objective lens provides a field of view of 430 μm. The nominal diffraction-limited lateral resolution is 0.6 μm and optical section thickness is 2 μm. The detection pinhole diameter is 150 μm, which corresponds to five times the nominal lateral resolution. The illumination laser beam is linearly polarized (*p*-state) and detection is through a cross-polarizer or analyzer (*s*-state). By rotation of a quarter-wave plate behind the objective lens, the illumination can be switched between brightfield and cross-polarized. Images are captured with a frame grabber (Imaq 1408, National Instruments Inc., Austin, Texas).

As in previous studies,[4,5,23,24] water as an immersion medium was often substituted with water-based gels such as Aquasonic 100 ultrasound gel and Suave® hair gel. These gels have refractive indices of 1.36 and 1.34, respectively, that

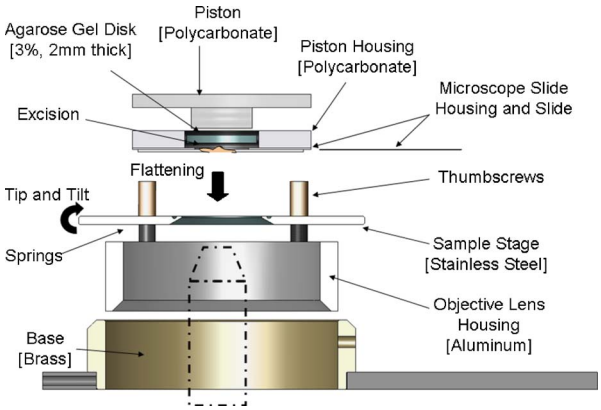

Fig. 1 Mechanical fixture to mount surgical skin excisions and enable mosaicing over large areas of tissue. The fixture encases the inverted objective lens.

are reasonably close to that (1.33) of water. Furthermore, the gels have a higher degree of viscosity and can therefore be placed on the inverted objective lens. By comparison to water, the use of these gels (particularly, Suave®) appeared not to degrade the image quality of the superficial tissue layer. The immersion gel is placed between the objective lens and the coverglass window, while the skin excision is kept hydrated with PBS. Once the excision was placed in the fixture, properly positioned and oriented, and the illumination power adjusted, confocal images and mosaics were obtained.

The surface of the excision was imaged. Because the frozen excision undergoes thawing, rinsing, acetowhitening, and mounting in the fixture, distortions in the imaged surface may occur due to the mechanical compliance of tissue. Thus, a close but not exact correspondence was expected between the confocal mosaics of the imaged surface and the sections of frozen histology that were prepared by the Mohs technician.

2.4 *Mechanical Tissue Fixture*

Fresh skin excisions from Mohs surgery are of complex and awkward 3-D shape and size, and are living and hydrated, and therefore not easy to mount for microscopy. To enable confocal mosaicing, to observe large fields of view covering large areas of the excision, we designed a mechanical fixture to hold the surgical excision and precisely control its flattening, tilt, sag, and stability (Fig. 1). The design of the fixture parallels the functionality of commercially available cryostats (for example, the CM1510 from Leica Microsystems Inc.) that are used for positioning and orienting Mohs surgical excisions prior to preparing frozen histology sections.

The tissue fixture (Fig. 1) accommodates the inverted objective lens configuration of the confocal reflectance microscope that uses the custom 30×, 0.9 NA water immersion objective lens, which images through a 1-mm-thick cover slide. Creating mosaics of a large area requires the fixture to gently flatten and accurately position and orient the lower surface of the excision that is to be imaged. This requires gentle and uniform pressure on the excision, with variable tilt and adjustable objective lens-to-excision distance. (In close analogy, proper positioning and orientation of the skin excision in the cryostat is a crucial task for Mohs technicians when preparing frozen histology sections.) Once the excision is placed on the glass window, a piston is used to apply pressure on the top to flatten the lower surface. The 1-mm-thick coverglass slide is stiff enough to prevent the lower surface (i.e., object plane to be imaged) from sagging under the pressure of the piston. (Standard 170-μm-thick microscope coverslips that are normally used with standard objective lenses do not work as well. The coverslips tend to sag or break such that capturing a 2-D sequence of images to create a mosaic over a large contiguous area is not possible.) The tilt and orientation of the window relative to the objective lens is adjusted via spring-loaded thumbscrews. (This is similar to the kinematic mount that is commonly used in optics.)

To ensure uniform pressure and uniform flattening of the lower surface, a mechanically compliant material is necessary between the piston and the irregular corrugated shape of the excision. We use cold-form agarose gel disks, prepared with concentration of 3% and thickness 2 to 3 mm. Agarose powder of 0.9 g is dissolved in 30 ml of hot water, placed in circular Delrin-plastic molds of 1.1875 in. diam and cooled to room temperature. Under the piston-induced pressure, the gel conforms to the shape of the excision, which then becomes embedded within the disk. (This is analogous to the embedding of skin excisions in the cryostat for preparing Mohs histology.) Agarose gel concentrations of 1 to 5% with disk thickness of 1 to 5 mm were tested. With concentrations of 1 and 2%, the disks were too fragile and broke under the pressure applied by the piston. With concentrations of 4 and 5%, the disks were too stiff and did not conform to the excision. Agarose gel disk concentration of 3% conformed to the excision without breaking. Disks with a thickness of 1 mm broke while those with thicknesses of 2 to 5 mm did not. This fixture encompasses the objective lens and is mounted onto the 3-D *xyz* translation stage of the reflectance confocal microscope with user-controlled height adjustment. The system is robust and enables accurate and repeatable imaging and mosaicing.

2.5 *Confocal Mosaicing*

Skin excisions from Mohs surgery are typically 10 to 20 mm in extent, whereas the confocal field of view with the current 30× objective lens is 0.43 mm. (More recently available lenses with lower magnification such as Nikon 20×/0.75 NA, Olympus 20×/0.95 NA, and Lucid 10×/0.8 NA provide increased fields of view of 0.75 to 1.00 mm.) To observe large areas of an excision, a rastered 2-D sequence of images is captured and stitched in software to create a mosaic that displays a much larger field of view. The rastered sequence of images is captured by translating the tissue fixture with stepper-motors-driven linear *XY* stages (Hayden Inc., Stamford, Connecticut). Individual images are captured using Vivascope software and mosaics are subsequently created with MATLAB software (Version 7.0.1, MathWorks, Natick, Massachusetts). The software routine consists of the following steps: (1) normalization of images with a reference background image, to correct for illumination curvature and vignetting, and (2) cropping of images at the four edges by 5 to 15%; the amount of cropping depends on the size of the excision, which necessitates a trade-off between amount of overlap and mosaicing speed; (3) merging or concatenation of the images into a single mosaic; (4) removal

of residual shading bands at the edges of each image with a reverse polynomial fit; (5) Fourier-transform-based removal of residual dark stitching lines; and (6) scaling down to resolution and pixelation that is equivalent to that in 2× magnified views of histology. (The mosaicing software and technical support is freely available to anyone who may be interested.) Currently, up to 36×36 images are stitched together to display a field of view of up to 12×12 mm, which simulates light microscope magnification of 2×. Mohs surgeons routinely use an objective lens with 2× magnification to quickly examine large areas of frozen histology sections during surgery. A continuous step-and-capture routine requires about 5 min for 36×36 frames.

When routinely examining frozen histology sections with a standard brightfield microscope, using a 2×, 0.08 NA objective lens and white-light illumination (wavelength λ ~0.5 μm), the Mohs surgeon observes a field of view of ~10 mm with a resolution of ~4 μm. The observed field of view consists of ~2500×2500 pixels, assuming 1 pixel per optical lateral resolution element. Thus, the confocal mosaics must be displayed with at least 2500×2500 pixels to ensure the display resolution does not degrade the optical lateral resolution. We observe mosaics on a 21-in. PC monitor (ViewSonic Corporation, Professional Series P220*f*, Walnut, California) using visualization software (PhotoImpact, MicroTek, or IPLab Spectrum version 3.0, Scanalytics Inc.). This software enables digital zooming to increase the display magnification to 4 or 10×, which mimics the Mohs surgeon's occasional *ad hoc* use of 4 or 10× objective lenses to examine histology with higher magnifications.

Each image consists of 640×480 pixels, is 8-bit gray scale, and requires ~1/4 MB of memory, such that a mosaic of 36×36 images at full resolution consists of more than 23,000×17,000 pixels and requires ~300 MB of memory. The mosaic is scaled down using bilinear interpolation, to make the final display equivalent to a histology-like 2× view. This display consists of ~2500×2500 pixels and requires ~4 MB.

2.6 *Preparation of Histology*

The frozen histology sections of each excision, which were prepared by routine hematoxylin and eosin (H&E) staining during Mohs surgery, were available for comparison to the confocal mosaics. The confocal images, mosaics, and submosaics were visually correlated to the histopathology at standard microscope magnifications (2 to 40×). As explained earlier, a close but not exact correlation to histology is expected.

3 Results

3.1 *Acetowhitening: Optimum Concentration and Soaking Time*

Figure 2 shows that a range of acetic acid concentrations at varying soaking times is effective for sufficiently brightening nuclei in acetowhitened excisions. Compared to controls, concentrations of 10 and 5% require only 30 s, whereas 3, 2, and 1% concentrations require 1, 2, and 5 min, respectively. Rapid brightening within 1 min is possible for concentrations of 3% and higher. The brightening of nuclei, as observed only on the exposed surface of the excision, is independent of the size of the excision for the acetic acid-to-skin excision volume ratio of 15:1.

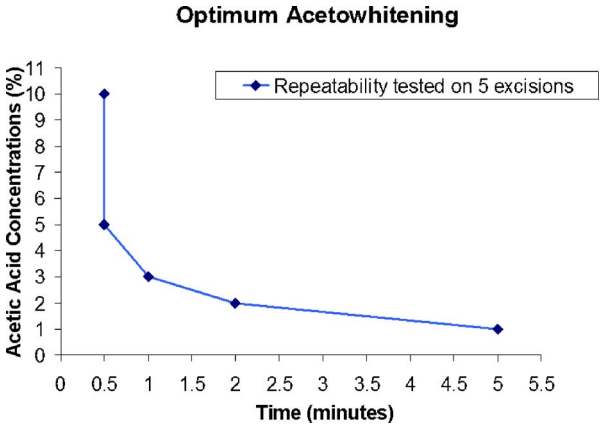

Fig. 2 Soaking time required at varying acetic acid concentrations. Concentrations of 10 and 5% require only 30 s, whereas 3, 2, and 1% concentrations require 1, 2, and 5 min, respectively. Rapid brightening within 1 min is possible for concentrations of 3% and higher. The brightening of nuclei on the surface is independent of the size of the excision for the acetic acid-to-skin excision volume ratio of 15:1. This observation of rapid acetowhitening is limited to only the exposed surface of the excision that was imaged.

3.2 *Confocal Mosaics: Visual Comparison to Histology*

Confocal mosaics of Mohs excisions show good visual correlation to frozen histology. The observed morphology of BCCs in terms of shape, size, and location of nests compares well to that in the corresponding histology. The atypical morphology of nuclei such as polymorphism (varying shapes and sizes), crowding (increased density), and palisading is clearly visualized in the mosaics.

Figure 3 shows a confocal mosaic of a micronodular BCC and the corresponding histology. Both the mosaic and the histology show nests of micronodular BCCs within the deeper reticular dermis [* in Figs. 3(A) and 3(B)]. The epidermal margin of the excision along with the dermo-epidermal junction can be differentiated (arrows). The acetowhitening clearly shows enhanced BCC-to-dermis contrast.

Figure 4 shows a submosaic of a superficial BCC at higher magnification of ~4×. Bright nuclear detail is more clearly visible in both the epidermis (arrows) and in the BCC within the underlying deeper dermis (*). The individual layers of the epidermis, namely, stratum corneum, granular, spinous, and basal cell layers, are seen.

Figure 5 shows a micronodular BCC in a smaller submosaic at higher magnification of 10×. Small nests of BCCs are seen in the deeper dermis (*) with bright nuclei. Again, the epidermis is seen with bright nuclei throughout (arrows). Within the dermis, nuclear detail in hair follicles near the dermo-epidermal junction is differentiated ["h" in Figs. 5(A) and 5(B)] along with individual inflammatory cells and collagen throughout the papillary and reticular dermis. The thin collagen fibers in the superficial papillary dermis and the

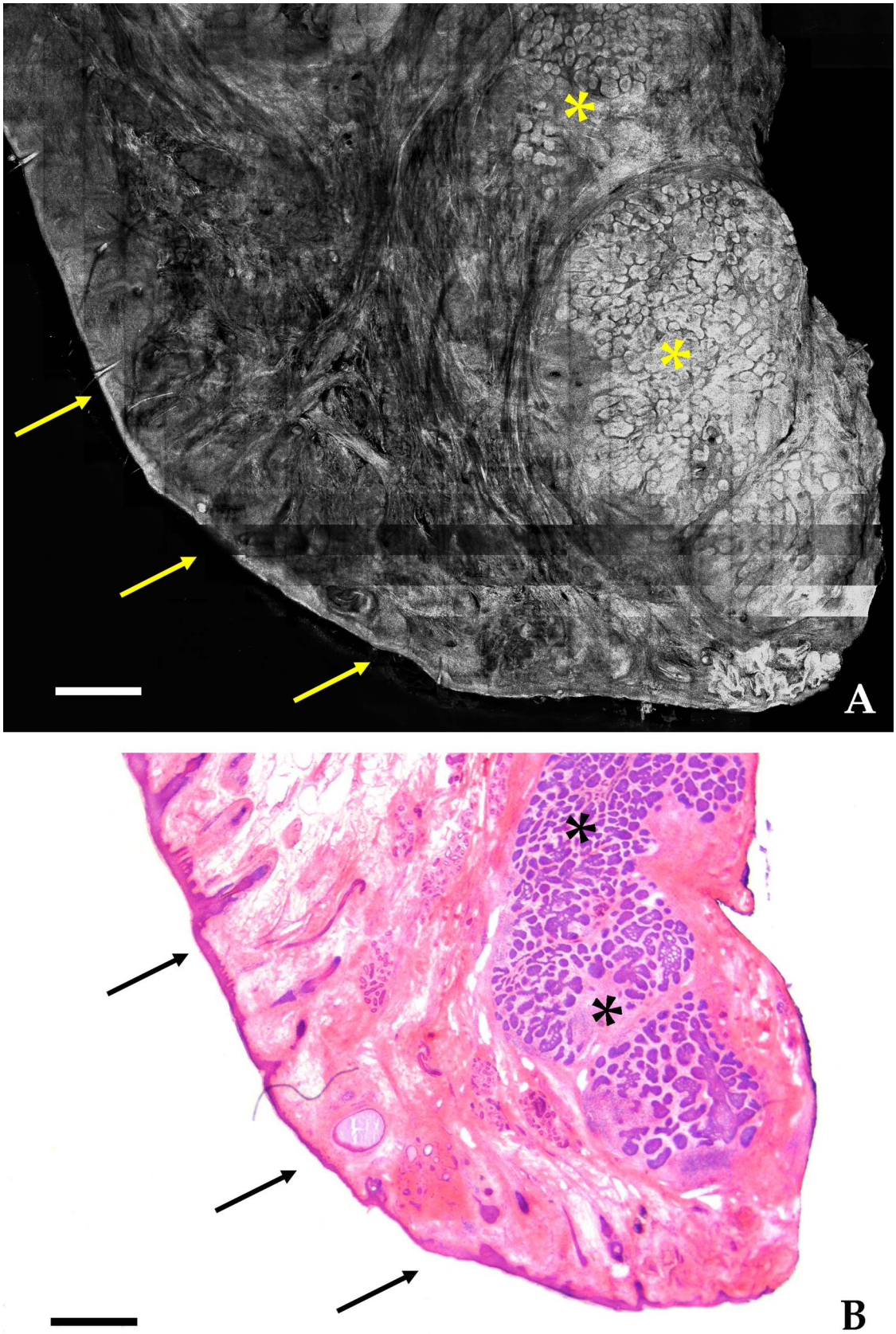

Fig. 3 (A) Mosaic shows 15×15 frames stitched together in software to show an equivalent 2×magnified view of the specimen. Within the dermis the clusters of micronodular BCCs are differentiated in the deep dermis because of brightening by the acetowhitening technique (*). The epidermis is seen along the superficial peripheral edge (arrows). Acetowhitening: 2% for 2 min. Scale bar 1 mm. (B) Corresponding frozen H&E stained histology showing correlation to the confocal mosaic. Scale bar 1 mm.

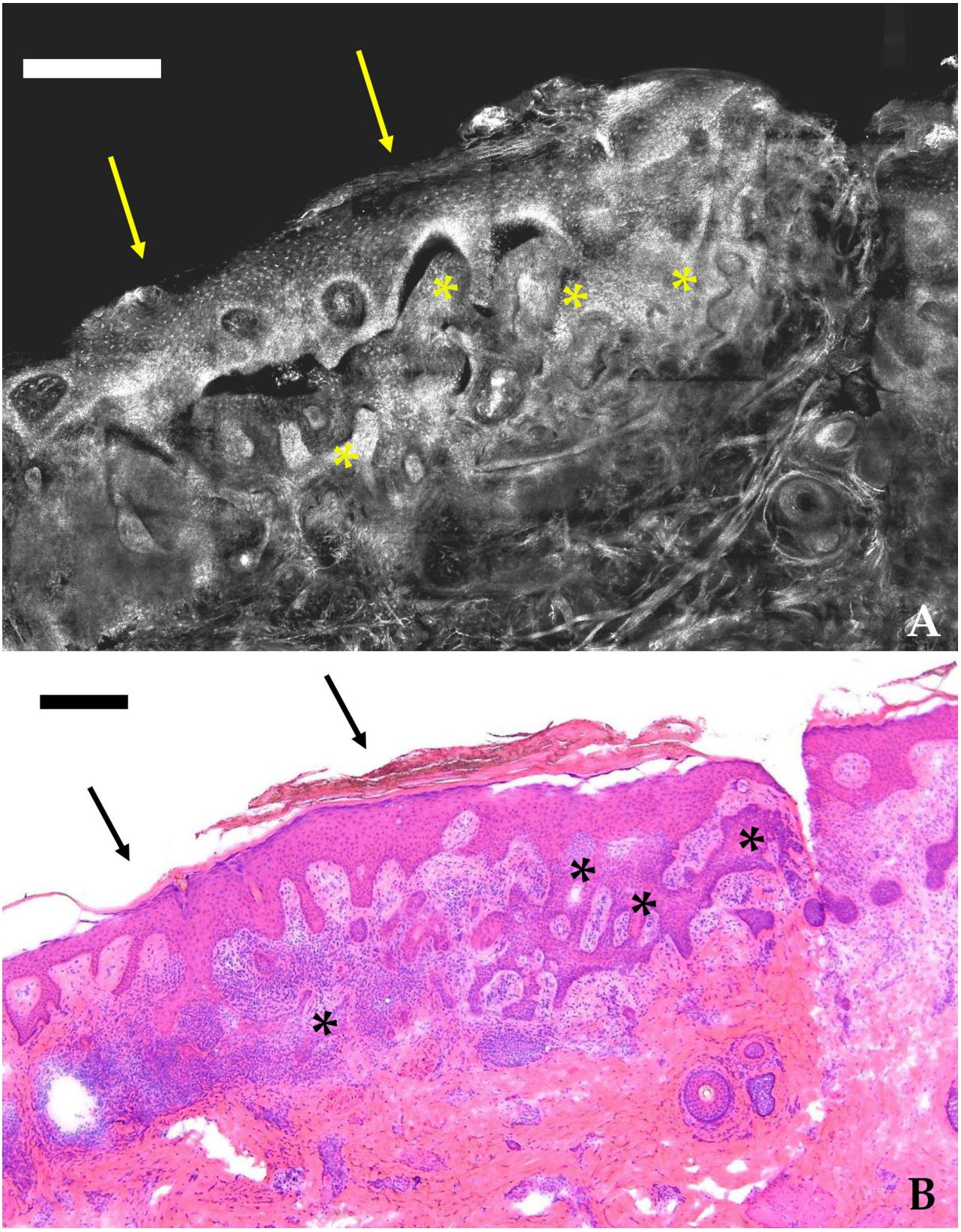

Fig. 4 (A) Confocal submosaic of a superficial BCC shows 8×6 frames stitched together to show an equivalent ~4× magnified view. Bright nuclei are more clearly seen in epidermis along the peripheral edge (arrows) and the BCC (*) in the underlying deep dermis. Acetowhitening: 3% for 1 min. Scale bar 500 μm. (B) Corresponding frozen H&E stained histology. Scale bar 500 μm.

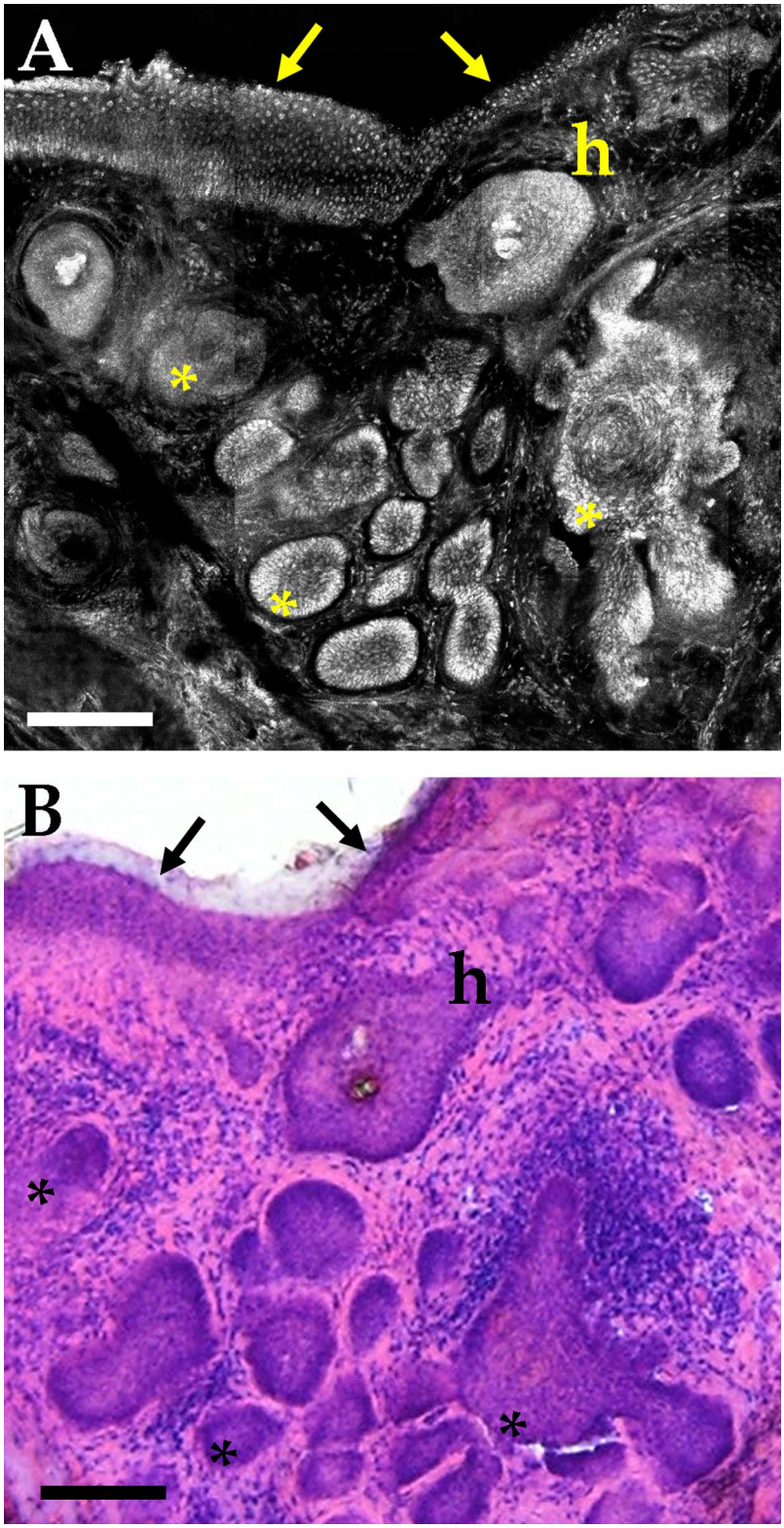

Fig. 5 (A) Confocal submosaic of micronodular BCC shown in 4×4 frames stitched together to show an equivalent 10× magnified view. The submosaic shows small nest of BCCs with bright nuclei (*), the epidermis along the edge (arrows), and bright nuclear detail in hair follicles (h). Bright nuclei of inflammatory cells are also seen infiltrating the dermis. Acetowhitening: 3% for 1 min. Scale bar 250 μm. (B) Corresponding frozen H&E stained histology. Scale bar 250 μm.

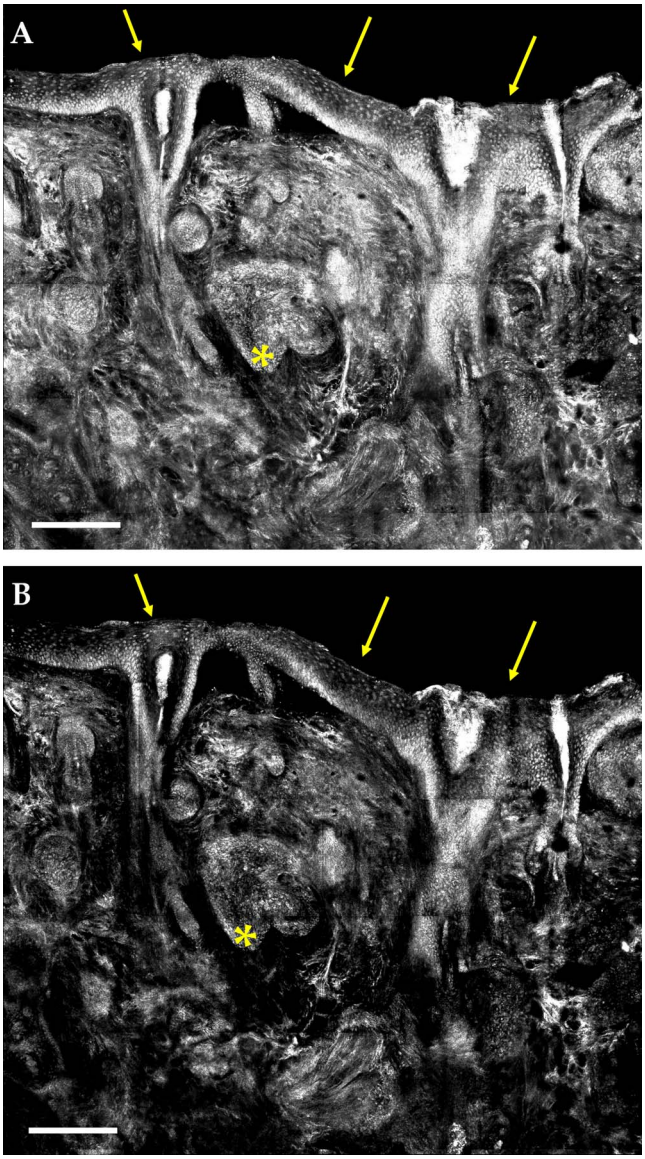

Fig. 6 Comparison of (A) brightfield versus (B) cross-polarized submosaics. Under cross-polarization, the brightness of the cytoplasm and the collagen is suppressed. Nuclei in the epidermis and the nests of BCCs appear with enhanced contrast. Scale bar 100 μm.

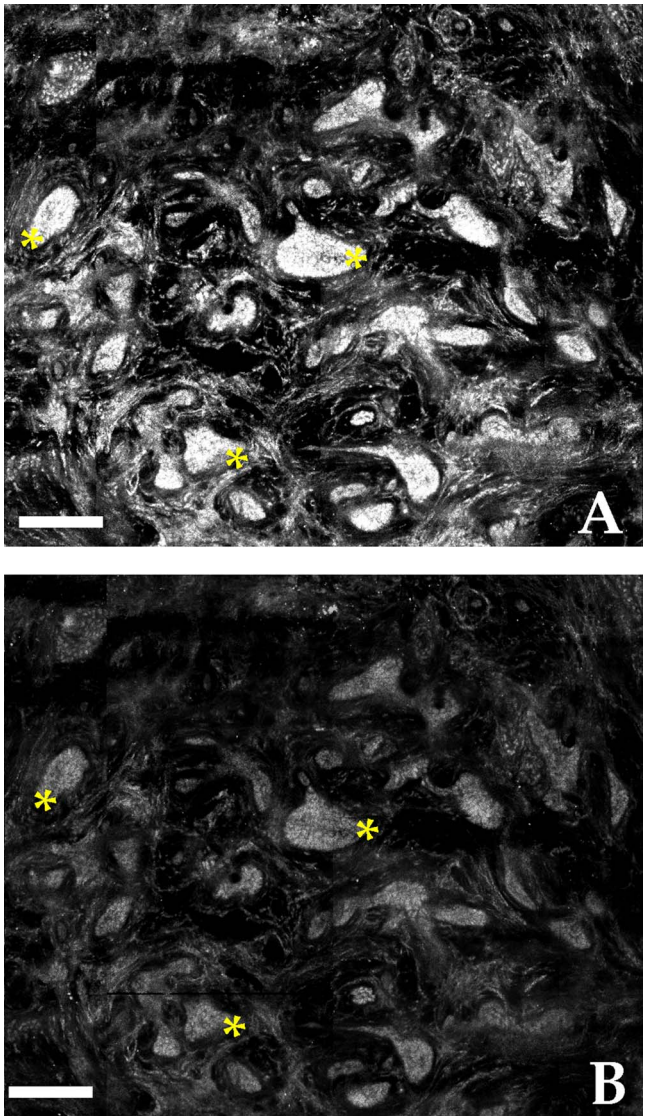

Fig. 7 Comparison of (A) brightfield versus (B) cross-polarized submosaics. Under cross-polarization, the brightness of the collagen is suppressed. Nuclei in the nests of BCCs appear with enhanced contrast. Scale bar 250 μm.

thicker collagen bundles in the deeper reticular dermis are seen in the mosaics, similar to that seen in the corresponding histology.

Tumor nests consisting of BCC cells mixed with inflammatory infiltrative cells are easily visualized in the confocal mosaics. Large nodular and small micronodular BCCs are easily detected in the mosaics and correlated to the frozen histology. However, infiltrative or sclerosing BCCs are difficult to detect because they consist of very small nests or thin strands of nuclei that tend to remain hidden within the bright collagen in the dermis.

3.3 *Comparison of Cross-polarized versus Brightfield Contrast*

A comparison of cross-polarized versus brightfield mosaics is shown in Figs. 6 and 7. The cross-polarized images show better overall contrast. Images obtained by cross-polarization suppress the light backscatter from the cytoplasm and dermis,[4] thereby increasing the contrast of nuclear detail relative to the dermis. Nuclei in the epidermis [arrows in Figs. 6(A) and 6(B)] and in the nests of BCCs [* in Figs. 6(A), 6(B), 7(A), and 7(B)] appear with enhanced contrast. Collagen within the superficial papillary dermis darkens consistently in cross-polarized images due to its homogeneous morphology. However, collagen does not consistently darken in the deeper reticular dermis due to the increased heterogeneity in terms of inherently thicker, denser, and more randomized arrangement of fibers and bundles. The enhancement of BCC-to-dermis contrast is thus consistent within the papillary dermis but not within the reticular dermis. The enhancement of contrast is better appreciated in individual images and submosaics at high magnification, rather than in the large mosaics at lower magnification. Cross-polarized mosaics do not neces-

sarily improve the detectability of BCCs in the deeper dermis, compared to brightfield mosaics.

4 Conclusions

The acetowhitening technique (i.e., soaking skin excisions in acetic acid) proved to be effective for brightening the nuclei, enhancing nuclei-to-dermis contrast, and improving detectability of BCCs. The acetowhitening does not affect subsequent frozen H&E histology of skin excisions for the purposes of making a diagnosis. Rapid brightening of nuclei, within 30 s, is possible with concentrations of acetic acid between 5 to 10%. The brightening of nuclei on the surface is independent of the size of the excision for the large (15:1) acetic acid-to-tissue volume ratio that was used. This observation of rapid acetowhitening is limited to only the exposed surface of the excision that was imaged. High concentrations of 5 to 10% may be used on skin excisions in future clinical applications for Mohs surgery. However, the lower concentrations of 1 to 3% may be more applicable for intraoperative imaging directly on the patient during surgery.

Confocal mosaics enable observation of large areas of the excision, up to 15×15 mm, equivalent to a $2\times$ view typically used by Mohs surgeons to examine frozen histology. To create mosaics, precise mechanical fixturing of the skin excisions is necessary, similar to the mounting of excisions in a cryostat used for preparing frozen histology sections. Currently, preparing a mosaic requires about 9 min compared to the 20 to 45 min required for preparing Mohs frozen histology.

Nuclear morphology of BCCs is detected in confocal mosaics when the display resolution (pixelation) equals or exceeds that of $2\times$-magnified histology that is commonly used by the Mohs surgeon. The correlation between the confocal mosaics and submosaics to the corresponding frozen histology at 2 to $4\times$ magnifications is accurate and repeatable in terms of shape, size, location and morphology of BCCs. Large nodular, smaller micronodular, and superficial BCCs are easy to detect. Infiltrative and sclerosing BCCs are not easily detected and tend to be obscured by the surrounding bright dermis. Cross-polarization darkens collagen in the dermis, enhances overall contrast and the appearance of mosaics, and minimizes optical artifacts. This improves detectability of BCCs in the superficial papillary but not in the deeper reticular dermis.

Further research is necessary to enhance the nuclei-to-dermis contrast and improve detectability of BCCs, especially for the infiltrative and sclerosing types. Correlation between mosaics and histology must be improved for both positive (i.e., presence of BCCs) and negative (i.e., absence of BCCs) cases. As with any new imaging modality, "image understanding" will be the most critical factor for developing confocal mosaicing into an accurate and repeatable method for detecting BCCs in skin excisions. In the long term, confocal reflectance mosaicing may prove useful to either guide Mohs surgery or as an adjunct to frozen histology.

Acknowledgments

The authors thank Marie Tudisco and Barbara Strippoli for the excised specimens from Mohs surgeries and technical help with frozen histology, Dr. Charles DiMarzio at Northeastern University and Dr. James Zavislan at the University of Rochester for their expertise in optics, and Dr. Jay Eastman and William Fox at Lucid Inc. for their technical support. This work is funded by National Institutes of Health (NIH) Grant No. R01EB002715 from the National Institute of Biomedical Imaging and Bioengineering's (NIBIB's) Image-Guided Intervention program (program officer Dr. John Haller).

References

1. A. Jemal, R. Siegel, E. Ward, T. Murray, J. Xu, C. Smigal, and M. J. Thun, "Cancer statistics, 2006," *CA-Cancer J. Clin.* **56**(2), 106 (2006).
2. F. Mohs, "Chemosurgery—a microscopically controlled method of cancer excision," *Arch. Surg. (Chicago)* **42**, 278–295 (1941).
3. K. G. Gross, H. K. Steinman, and R. P. Rapini, *Mohs Surgery: Fundamentals and Techniques*, pp. 1–10, Mosby, St. Louis (1999).
4. M. Rajadhyaksha, G. Menaker, T. Flotte, P. J. Dwyer, and S. González, "Confocal examination of nonmelanoma cancers in thick skin excisions to potentially guide mohs micrographic surgery without frozen histopathology," *J. Invest. Dermatol.* **117**(5), 1137 (2001).
5. V. Q. Chung, P. J. Dwyer, K. S. Nehal, M. Rajadhyaksha, G. M. Menaker, C. Charles, and S. B. Jiang, "Use of *ex vivo* confocal scanning laser microscopy during Mohs surgery for nonmelanoma skin cancers," *Dermatol. Surg.* **30**(12, Pt.1), 1470 (2004).
6. Z. Tannous, A. Torres, and S. González, "*In vivo* real-time confocal reflectance microscopy: a noninvasive guide for Mohs micrographic surgery facilitated by aluminum chloride, an excellent contrast enhancer," *Dermatol. Surg.* **29**(8), 839 (2003).
7. D. E. Marra, A. Torres, C. F. Schanbacher, and S. Gonzalez, "Detection of residual basal cell carcinoma by *in vivo* confocal microscopy," *Dermatol. Surg.* **31**(5), 538 (2005).
8. A. Gerger, M. Horn, S. Koller, W. Weger, C. Massone, B. Leinweber, H. Kerl, and J. Smolle, "Confocal examination of untreated fresh specimens from basal cell carcinoma: implications for microscopically guided surgery," *Arch. Dermatol.* **141**(10), 1269 (2005).
9. J. Strasswimmer, M. C. Pierce, B. H. Park, V. Neel, and J. F. de Boer, "Polarization-sensitive optical coherence tomography of invasive basal cell carcinoma," *J. Biomed. Opt.* **9**(2), 292 (2004).
10. A. N. Yaroslavsky, V. Neel, and R. R. Anderson, "Demarcation of nonmelanoma skin cancer margins in thick excisions using multispectral polarized light imaging," *J. Invest. Dermatol.* **121**(2), 259 (2003).
11. A. N. Yaroslavsky, J. Barbosa, V. Neel, C. DiMarzio, and R. R. Anderson, "Combining multispectral polarized light imaging and confocal microscopy for localization of nonmelanoma skin cancer," *J. Biomed. Opt.* **10**(1), 14011 (2005).
12. E. Pickwell, A. J. Fitzgerald, B. E. Cole, P. F. Taday, R. J. Pye, T. Ha, M. Pepper, and V. P. Wallace, "Simulating the response of terahertz radiation to basal cell carcinoma using *ex vivo* spectroscopy measurements," *J. Biomed. Opt.* **10**(6), 064021 (2005).
13. R. M. Woodward, V. P. Wallace, R. J. Pye, B. E. Cole, D. D. Arnone, E. H. Linfield, and M. Pepper, "Terahertz pulse imaging of *ex vivo* basal cell carcinoma," *J. Invest. Dermatol.* **120**(1), 72 (2003).
14. V. P. Wallace, A. J. Fitzgerald, S. Shankar, N. Flanagan, R. Pye, J. Cluff, and D. D. Arnone, "Terahertz pulsed imaging of basal cell carcinoma *ex vivo* and *in vivo*," *Br. J. Dermatol.* **151**(2), 424 (2004).
15. L. M. McIntosh, M. Jackson, H. H. Mantsch, M. F. Stranc, D. Pilavdzic, and A. N. Crowson, "Infrared spectra of basal cell carcinomas are distinct from non-tumor-bearing skin components," *J. Invest. Dermatol.* **112**(6), 951 (1999).
16. A. Nijssen, T. C. Bakker Schut, F. Heule, P. J. Caspers, D. P. Hayes, M. H. Neumann, and G. J. Puppels, "Discriminating basal cell carcinoma from its surrounding tissue by Raman spectroscopy," *J. Invest. Dermatol.* **119**(1), 64 (2002).
17. C. af Klinteberg, A. M. Enejder, I. Wang, S. Andersson-Engels, S. Svanberg, and K. Svanberg, "Kinetic fluorescence studies of 5-aminolaevulinic acid-induced protoporphyrin IX accumulation in basal cell carcinomas," *J. Photochem. Photobiol., B* **49**(2–3), 120 (1999).
18. B. Stenquist, M. B. Ericson, C. Strandeberg, L. Mölne, A. Rosén, O. Larkö, and A. M. Wennberg, "Bispectral fluorescence imaging of aggressive basal cell carcinoma combined with histopathological

mapping: a preliminary study indicating a possible adjunct to Mohs micrographic surgery," *Br. J. Dermatol.* **154**(2), 305 (2006).
19. M. B. Ericson, J. Uhre, C. Strandeberg, B. Stenquist, O. Larkö, A.-M. Wennberg, and A. Rosén, "Bispectral fluorescence imaging combined with texture analysis and linear discrimination for correlation with histopathologic extent of basal cell carcinoma," *J. Biomed. Opt.* **10**(3), 034009 (2005).
20. S. Andersson-Engels, G. Canti, R. Cubeddu, C. Eker, C. af Klinteberg, A. Pifferi, K. Svanberg, S. Svanberg, P. Taroni, G. Valentini, and I. Wang, "Preliminary evaluation of two fluorescence imaging methods for the detection and the delineation of basal cell carcinomas of the skin," *Lasers Surg. Med.* **26**(1), 76 (2000).
21. L. Brancaleon, A. J. Durkin, J. H. Tu, G. Menaker, J. D. Fallon, and N. Kollias, "*In vivo* fluorescence spectroscopy of nonmelanoma skin cancer," *Photochem. Photobiol.* **73**(2), 178 (2001).
22. M. Rajadhyaksha, S. Gonzalez, and J. M. Zavislan, "Detectability of contrast agents for confocal reflectance imaging of skin and microcirculation," *J. Biomed. Opt.* **9**(2), 323 (2004).
23. M. Rajadhyaksha, M. Grossman, D. Esterowitz, R. H. Webb, and R. R. Anderson, "In vivo confocal scanning laser microscopy of human skin: melanin provides strong contrast," *J. Invest. Dermatol.* **104**(6), 946 (1995).
24. M. Rajadhyaksha, S. González, J. M. Zavislan, R. R. Anderson, and R. H. Webb, "In vivo confocal scanning laser microscopy of human skin II: advances in instrumentation and comparison with histology," *J. Invest. Dermatol.* **113**(3), 293 (1999).